Received: 24 March 2023 | Accepted: 25 May 2023

DOI: 10.1111/gcb.16847

Global Change Biology WILEY

RESEARCH ARTICLE

Observed forest trait velocities have not kept pace with hydraulic stress from climate change

G. R. Quetin[1] | L. D. L. Anderegg[2] | I. Boving[2] | W. R. L. Anderegg[3] | A. T. Trugman[1]

[1]Department of Geography, University of California, Santa Barbara, California, USA

[2]Department of Ecology, Evolution, and Marine Biology, University of California, Santa Barbara, California, USA

[3]School of Biological Sciences, University of Utah, Salt Lake City, Utah, USA

Correspondence
G. R. Quetin, Department of Geography, University of California, Santa Barbara, CA 93016, USA.
Email: gquetin@ucsb.edu

Funding information
National Science Foundation, Grant/Award Number: 2003205, 2017949 and 2216855; U.S. Department of Agriculture, Grant/Award Number: 2018-67012-31496

Abstract

The extent to which future climate change will increase forest stress and the amount to which species and forest ecosystems can acclimate or adapt to increased stress is a major unknown. We used high-resolution maps of hydraulic traits representing the diversity in tree drought tolerance across the United States, a hydraulically enabled tree model, and forest inventory observations of demographic shifts to quantify the ability for within-species acclimation and between-species range shifts to mediate climate stress. We found that forests are likely to experience increases in both acute and chronic hydraulic stress with climate change. Based on current species distributions, regional hydraulic trait diversity was sufficient to buffer against increased stress in 88% of forested areas. However, observed trait velocities in 81% of forested areas are not keeping up with the rate required to ameliorate projected future stress without leaf area acclimation.

KEYWORDS
biogeography, climate change, forest range shifts, plant water stress, tree mortality

1 | INTRODUCTION

Biogeographic range boundaries are highly visible outcomes of ecosystem functionalities due to spatial variations in climate and other limiting resources. However, the fundamental mechanisms controlling tree species distributions and range boundaries are still poorly understood, despite over two centuries of study (Anderegg & HilleRisLambers, 2019; Colwell et al., 2008; Louthan et al., 2015; MacArthur, 1984; Von Humboldt & Bonpland, 2010). Understanding the mechanisms regulating forest range dynamics is urgent, given that climate change has already caused widespread shifts in tree species' geographic extents across multiple biomes (Chen et al., 2011; Colwell et al., 2008; Esquivel-Muelbert et al., 2019; Lenoir et al., 2008), and it is expected that hotter droughts with further climate change have the potential to cause widespread declines in forest productivity and increases in mortality (Park Williams et al., 2013). A continuation or escalation of the observed trends could cause drastic range shifts or biome collapses (Cano et al., 2022; Cox et al., 2000) and flip the terrestrial carbon sink to a carbon source (Adams et al., 2010; Kurz et al., 2008).

There are several mechanisms by which tree species and forested communities can compensate for intensifying water stress associated with climate change. At the species level, one such mechanism that can mitigate stress is the coordinated adjustments in plant biomass allocation, such as adjustments in root or leaf allocation (Barton & Montagu, 2006; Mackay et al., 2020). Here, we focus on widely documented adjustments of leaf area relative to sapwood area (referred to subsequently as "adjustment in leaf area") within the same species across climate gradients such that individuals within a species decrease water demand (leaf area) relative to supply (sapwood area) in drier locations or seasons (Anderegg et al., 2021;

Martínez-Vilalta et al., 2009; Mencuccini & Grace, 1995; Piñol & Sala, 2000; Rosas et al., 2019). Various other physiological adjustments can buffer against drought stress within a species (e.g., local adaptation or acclimation of more embolism-resistant xylem or leaf tissue, deeper roots, etc.), but we focus on adjustments in leaf area here because allocation traits generally show much larger within-species variation than most other drought-related traits (Anderegg, Griffith, et al., 2022; Trugman, Anderegg, Sperry, et al., 2019).

At the community or stand level, there can be shifts in composition toward species with more drought-resistant plant hydraulic traits that can buffer a forest against water stress (Allen & Breshears, 1998; García-Valdés et al., 2021; Trugman et al., 2020). Finally, it is possible for biogeographic shifts to occur where more drought-resistant species expand their ranges to new stands over longer time horizons, provided that sufficient hydraulic trait reservoirs are available from proximal seed sources (Peters et al., 2015). These species shifts may take decades during which ecosystem services and forest carbon storage will decline (Seidl & Turner, 2022).

Trait-based vegetation models simulate the physiological processes hypothesized to be fundamental in governing terrestrial ecosystem responses to the variation of climate across space and climate change in the future, while being able to connect organ-level hydraulic traits measured in the field to organism- and ecosystem-level function. Yet few vegetation models incorporate the appropriate processes to test the extent to which shifts in leaf allocation within a species (Trugman, Anderegg, Wolfe, et al., 2019) or biogeographic changes in species composition may ameliorate climate-induced changes in forest stress. Here, we tested the extent to which changes in species biogeographic ranges, shifts in species relative abundance, and adjustment in leaf area within a species can compensate for increases in water stress with climate change. We used an optimization-based model of tree gas exchange, hydraulic transport, and leaf carbon allocation (Figure S1). The model was parameterized with current forest hydraulic trait distributions for the continental United States based on US Forest Inventory and Analysis data, tree height, and canopy efficiency (Trugman et al., 2020; Figures S2–S5) and forced with historical (1995–2014) and future (2081–2100) daily climate data (Figures S6 and S7).

We developed a new method for representing species diversity and within-species acclimation in a parsimonious plant functional type framework applicable to large-scale terrestrial biosphere models (see Section 2) and tested the extent to which trait acclimation and biogeographic shifts in community trait composition can ameliorate climate stress. Specifically, we asked: (i) How do hydraulic traits mediate plant stress and productivity across biogeographic and climate gradients of US forests? (ii) Are there systematic changes in stress with projected changes in climate and increased atmospheric CO_2 across forest biogeographies and climates? (iii) Where do projected stress levels increase or decrease with climate change in US forests? (iv) To what extent do within-species adjustments in leaf area alter the effects of climate stress? (v) To what extent and where can current trait reservoirs help forests avoid increases in water stress through biogeographic shifts in species compositions?

2 | MATERIALS AND METHODS

We used the HOTTER model (the Hydraulic Optimization Theory for Tree and Ecosystem Resilience model; Mathias & Trugman, 2022; Trugman, Anderegg, Wolfe, et al., 2019; Figure S1), a physiologically based tree model with a realistic representation of gas exchange (Eller et al., 2018) and a detailed representation of plant hydraulics (Trugman et al., 2018) to quantify spatial variations in tree water status, hydraulic stress, and carbon gain across gradients in climate and plant traits in the continental United States. Our model experiments combined hydraulic trait maps based on high-resolution species distribution and abundance data derived from the US Forest Service Forest Inventory and Analysis Program with a large hydraulic trait database (Trugman et al., 2020), tree height measured remotely by satellite, and daily historical and future climate forcing data (see Section 2). This combination of physiological traits and climate shaped the geographical distribution of hydraulic stress and carbon gain in trees for present-day conditions (1995–2014) and their response to future conditions (2081–2100).

2.1 | HOTTER model description

HOTTER combines key physiological processes of photosynthesis, autotrophic respiration, and plant hydraulics to simulate plant water status, carbon gain, and hydraulic stress. Here, we updated previous versions of the model (Mathias & Trugman, 2022; Trugman et al., 2018), to include a new stomatal optimization, the Stomatal Optimization Based on Xylem Hydraulics (SOX) (Eller et al., 2018). In this new version, stomatal behavior is governed by a leaf scale trade-off between the carbon gain of assimilation and a cost function based on the percent loss of conductivity in the tree xylem. The stomatal model was chosen to allow investigation of the response of the tree hydraulics to variations in traits and under future climate conditions.

HOTTER model meteorological forcings include atmospheric CO_2 concentrations (CO_2, ppm), temperature (T, C°), vapor pressure deficit (VPD, Pa), and soil water potential (ψ_{soil}, MPa). In addition, the tree model requires inputs or allometric equations for the state of the tree, leaf area (al, m^2), height (h, m), and diameter at breast height (dbh, cm^2). In these experiments, we use an observed dataset of height as an input, determine dbh via allometry, and determine leaf area through an optimization that maximizes net primary productivity (NPP) over a given time period (Figures S4, S5, S8; see Section 2.1.3 for details). The hydraulic dynamics of the model are primarily controlled by three plant physiological traits: the water potential and 50% loss of conductivity (P50, MPa); a slope parameter (b2 in the model) which governs how plant conductivity decreases with increased water stress (e.g., more negative plant water potentials); and the conductivity of the roots, xylem, and petioles (K_{max}, mmol H_2O m^{-1} s^{-1} MPa^{-1}). In our experiment, we set the P50 values based on the maps (Trugman et al., 2020, p. 20) (Figure S2), kept the slope parameter fixed for parsimony, and determine the K_{max} using an empirical function representing a safety versus efficiency trade-off where higher conductivity values are associated with less negative (i.e., more vulnerable to hydraulic stress) P50 values (Figure S3). For the

entire experiment, we used an observed relationship between P50 and K_{max} derived from Liu, Ye, et al. (2021) for angiosperms, which included the most observations and was broadly similar to gymnosperms.

HOTTER represents a tree canopy as a single leaf layer without shading and assumes that under average growth conditions, the two limiting photosynthetic rates should be equal resulting in a "maximum canopy efficiency" (Figure S5; Smith et al., 2019; Trugman, Anderegg, Wolfe, et al., 2019; Walker et al., 2014; see Section 2.1.2 for further details). The canopy efficiency is sensitive to temperature through a fixed Q_{10} response to temperature (Mathias & Trugman, 2022).

Finally, each tree organ, including leaf area, xylem, phloem, and roots, includes respiration that is also sensitive to temperature through a fixed Q_{10} response to temperature (Mathias & Trugman, 2022). The combination of these respiration terms, a 30% growth respiration, and carbon assimilation through photosynthesis allowed the model to predict gross primary productivity (GPP), autotrophic respiration (Rh), and the difference between the two—net primary productivity (NPP)—in different climates and for different traits and states of trees. Additionally, HOTTER diagnostic outputs include tree-level transpiration (Tr), and the water potential (ψ) and percent loss of conductivity (PLC) for all of the tree's conductive elements: roots, xylem, and leaves. Model outputs are daily level and assume 12 h of daylight for carbon assimilation during the growing season and 24 h of respiration. See Table S1 for a summary of HOTTER parameterizations and outputs.

2.1.1 | Incorporation of a cost–gain stomatal representation

The SOX stomatal model has shown skill in simulating stomatal responses to drought (Eller et al., 2018, p. 202) and cost–gain models have been developed to represent the hydraulic changes observed in the field (Anderegg et al., 2018; Sabot et al., 2022; Sperry et al., 2016, 2017; Venturas et al., 2017, 2018; Wang et al., 2020). Our implementation of the SOX model uses the PLC of the xylem to represent the cost function (k_{xylem}) and the assimilation rate (A) in the tree model to represent the gain function. Then for each daily time step, the optimal internal CO_2 concentration, and thus stomatal conductance, to maximize the gain–cost function is determined (Equation 1).

$$\frac{\partial\left(A \cdot k_{xylem}\right)}{\partial\left(c_i\right)} = 0 \quad (1)$$

to capture the dynamics from "leaky stomata" (Machado et al., 2021), we have included a minimum stomatal conductance of 0.002 mol m^{-2} s^{-1} (Bonan, 2002, p. 246). Optimization was performed using the Scipy minimize function "fmin" (Virtanen et al., 2020).

2.1.2 | Canopy efficiency

As a simplification, a tree canopy in HOTTER is comprised of a single leaf layer and it is assumed that two limiting photosynthetic rates (i.e., the photosynthetic rate limited by the maximum rate of Rubisco carboxylation and the photosynthetic rate limited by the electron transport rate for the regeneration of ribulose-1,5,-bisphosphate) should be equal according to Smith et al. (2019), resulting in a "maximum canopy efficiency" under average growing conditions. For the calculation of canopy efficiency, we used a spatially varying climatology during the growing season of insolation created from daily data (Figure S6d). Canopy efficiency is sensitive to temperature as in Mathias and Trugman (2022). Scaling productivity from the leaf to the canopy scale is accomplished by multiplying leaf scale productivity by total leaf area (Figure S5). Note that this scaling includes the simplifying assumption of zero shading between leaves in the canopy.

2.1.3 | Leaf area optimized for maximizing carbon gain

In all model experiments, the leaf area of the model tree in each climate grid cell was determined through optimizing tree carbon gain (i.e., the NPP) to maximize integrated NPP over the 20-year simulation period (either 20-year historical or future climate period). As leaf area increased so did productivity (through the increased canopy size) but the carbon loss through respiration from leaves, stem, and roots (determined as proportional to canopy size) also increased. In addition, greater leaf areas increase transpiration, which increases hydraulic stress for a given ψ_{soil}, triggering stomatal closure. The balance of these opposing mechanisms led to a unique (i.e., determinable through optimization) leaf area for maximizing carbon gain. The optimization was performed using the SciPy optimization package in Python (Virtanen et al., 2020). The optimization method used was the "Nelder–Mead" with maximum iterations of 20 and a leaf area tolerance of 0.2.

2.2 | Data sources

2.2.1 | Daily meteorology (1995–2014)

Daily mean meteorology, including soil water potential, temperature, and vapor pressure deficit, from the NASA Global Land Data Assimilation System Version 2 (GLDAS-2) was used as model forcing for the tree model (specifically, GLDAS Catchment Land Surface Model L4 daily 0.25×0.25-degree GRACE-DA1 V2.2 [GLDAS_CLSM025_DA1_D_2.2] Li et al., 2019, 2020; Figure S6). The GLDAS-2 data are a combination of satellite and ground-based observations assimilated into land surface models. The data were primarily chosen because of a track record of use in modeling the land surface, relatively high spatial resolution (0.25°), and a daily time resolution which enabled model predictions for day-to-day variations in water stress. While the uncertainty due to meteorology is not explored here, previous work predicting carbon fluxes has shown that the choice of driving meteorology can lead to variations of 9% in global gross primary productivity (Wu et al., 2017). The data can be downloaded from https://disc.gsfc.nasa.gov/.

The vapor pressure deficit was calculated from daily mean values of temperature and specific humidity. Soil water potential was calculated from root zone soil water content based on Campbell (1974) as implemented in Mathias and Trugman (2022).

2.2.2 | Tree height

We determined tree height as a model input from remote-sensed observations of tree height from the Global Ecosystem Dynamics Investigation (GEDI) instrument and processed by the Global Land Analysis and Discover team at the University of Maryland (Potapov et al., 2021). The data are a snapshot of tree height from April to October 2019. The native resolution was 0.00025×0.00025 degree and we re-binned the data to the 0.25×0.25-degree grid of the meteorology. Re-binning was performed through an area-weighted mean of the higher resolution observations to the coarser grid (Figure S4). Note that while the coarsened mean values are representative of each larger pixel, the native high resolution of the dataset shows there is also variability in height. This variability represents another dimension of uncertainty and potential acclimation not directly investigated in this paper (Figure S4b). In addition, absolute uncertainty is likely to increase in tall dense forests such as the Pacific Northwest and Northeast (Liu, Cheng, & Chen, 2021). Data are available from https://glad.umd.edu/dataset/gedi/.

2.2.3 | CMIP6 downscaled future meteorology

To create a future climate scenario, the monthly changes in temperature and relative humidity from the Coupled Model Intercomparison Project Phase 6 (CMIP6) (Eyring et al., 2016) climate models run for the SSP 3-7.0 emissions scenario (the medium to high end of the range of future forcing pathways in CMIP6) were combined with the daily GLDAS-2 meteorological data to create daily values for the future. The CMIP6 models included in the analysis were ACCESS-CM2, ACCESS-ESM1-5, CanESM5-CanOE, MIROC-ES2L, MPI-ESM1-2-LR, and MRI-ESM2-0THE. Downscaled model products publicly available (Anderegg, Chegwidden et al., 2022) were used.

Monthly climatology of each CMIP6 model's temperature mean and relative humidity were calculated for each grid cell for a historical period (1985–2014) and for the SSP 3-7.0 future scenario (2081–2100). The median values of these climatology were then calculated across the suite of six models to reduce biases represented in any one model. We employed the "delta" method to bias correct the climate data (Navarro-Racines et al., 2020) such that the difference between these future and historical periods was added to the daily values from GLDAS-2 to create daily data with mean monthly changes reflective of monthly average conditions during 2081–2100. For temperature, the new data were created through a simple addition of the monthly temperature delta to each daily value of temperature. To better account for the nonlinearity of vapor pressure deficit in creating a future dataset, the relative humidity for each time period was first converted to specific humidity before calculating a delta between the time periods. This monthly delta in specific humidity was then added to the daily specific humidity derived from GLDAS-2. Finally, a new daily vapor pressure deficit was calculated from the new daily values of future temperature and specific humidity. Note that while this method allows us to investigate changes in mean climate variables along SSP 3-7.0, it does not account for potential changes in climate variability with climate change. While this work focuses on decadal trends in climate, future work on increases in variance and the frequency of extreme drought events could explore the impact of changes to water stress events.

2.2.4 | Atmospheric concentrations of CO_2

A constant atmospheric concentration of CO_2 was used for both the present-day (1995–2014) and future (2081–2100) experiments. The constant values were averages of the observations at Mauna Loa (370 ppm) (Keeling et al., 2009, 2017) for the present day and taken from the CMIP6 SSP 3-7.0 emissions scenario for the future (753 ppm; O'Neill et al., 2016).

2.2.5 | Hydraulic traits

The P50 maps used to parameterize the tree model across the continental United States are derived from Trugman et al. (2020), who used the USDA Forest Inventory and Analysis program (FIA) plot inventory data and a global database of species-level P50 measurements. For this study, the maps from Trugman et al. (2020) were gridded to 0.25° to reflect the same spatial scale as that of the meteorological forcing. We calculated several metrics of ecosystem diversity at the grid cell level designed to be reflective of commonly used diversity metrics in ecosystem ecology representing alpha, beta, and gamma diversity. First, we calculated the grid-level mean community-weighted (CW) mean P50 (weighted in each plot by species basal area, see Trugman et al. (2020)) based on all plots within a grid cell. We also calculated minimum and maximum plot CW P50 observed in the grid cell (CW least/most vulnerable). In addition, for each plot, we calculated the minimum and maximum P50 of species present in the plot and then calculated the grid-average min/max P50 across plots (plot least/most vulnerable). This was intended to characterize the maximum trait change that could be accomplished by changes in species relative abundance within a plot, without colonization of new species. Finally, we calculated the min/max P50 values using any species occurring in any plot within the grid cell (region least/most vulnerable; Figure S2) to represent the total possible trait diversity of species present in a grid cell that could plausibly disperse to plots. Collectively, HOTTER model experiments with these complementary metrics of trait diversity enabled us to quantify the extent to which shifts in forest composition toward species with more drought-resistant species can accommodate climate stress and the extent to which range expansion of drought-resistant species may mitigate forest loss due to increased climate stress.

The P50 values were used to determine the maximum conductivity value of the tree (K_{max}) through observations of the safety versus efficiency trade-off where lower values of P50 are accompanied by lower values of maximum conductivity (Figure S3). Here, we used the trade-off fit to angiosperm observations determined in Liu, Ye, et al. (2021) which had the most observations and were similar to gymnosperm.

2.2.6 | SPEI drought index

The Standardized Precipitation Evapotranspiration Index provides an integrated drought index for comparison with modeled predictions (Vicente-Serrano et al., 2010). SPEI indicates a departure from a baseline climate and is thus relative to climate at each spatial point. The relative nature of SPEI can capture the water stress in trees caused by an abnormally dry year. The growing season (June, July, August) from the years 2000–2015 were used in this analysis and interpolated to the model resolution of 0.25° latitude longitude with a linear interpolation. The data were downloaded from https://spei.csic.es/database.html on 11.18.2023.

2.2.7 | Climatological water deficit

Climatological water deficit was used to determine dry regions (greater than 100 mm average monthly deficit during the growing season (June, July, August)) and wet regions (<100 mm average monthly deficit during the growing season (June, July, August)). We used the climatology of climatological water deficit from TerraClimate calculated between 1981 and 2010 and regridded through linear interpolation to the 0.25 degree HOTTER resolution (Abatzoglou et al., 2018). The data were downloaded as a netCDF from http://thredds.northwestknowledge.net:8080/thredds/catalog/TERRACLIMATE_ALL/summaries/catalog.html on 02/13/2023.

2.2.8 | HOTTER model validation

HOTTER has been validated against observational data of leaf area adjustment (Trugman, Anderegg, Wolfe, et al., 2019) and plant carbon balance (Mathias & Trugman, 2022). In addition, we find that present hydraulic stress in our runs with HOTTER (as represented by the 90th percentile of PLC and the stressed seasons experienced from 1995 to 2014) show skill in separating regions with high tree mortality for both dry and wet regions (Figure 3). To test this separation, we performed the Mann–Whitney *U*-test (test for difference in distributions) (Mann & Whitney, 1947) and the *t*-test (difference in mean values) (Yuen, 1974) between the observed mortality in two bins of HOTTER hydraulic stress. The SciPy package in python was used to perform both tests (Virtanen et al., 2020; see Table S2). This relationship between modeled hydraulic stress and mortality, along with previous model validation, supports the utility of HOTTER in exploring the present-day and future hydraulic stress of forests in the contiguous United States. In addition, HOTTER shows an increased ability to separate areas of mortality versus other points when compared with the purely climate-driven SPEI index (Figure 3).

2.2.9 | Change in percent loss of hydraulic conductivity

Where the percent loss in hydraulic conductivity (PLC) is reported, we use the 90th percentile calculated on the time series of days to highlight the days with higher stress as well as the difference between 90th percentiles in the present and future. To match this, we also report the 10th percentile (most stressed) days of the leaf water potential in Figure 1. For the present-day histograms, we present only the days more negative (greater) than the 10th (90th) percentile for water potential (PLC) (Figure 1; Figure S9). For the difference with the future, we present the difference between days that are more negative (greater) than the 10th (90th) percentile for water potential (PLC) (Figure 1; Figure S9).

2.2.10 | Defining a hydraulically stressed season

Here, we defined a season with potentially damaging hydraulic stress as a season with any 1 day exceeding a PLC >50%. In the present-day runs, we found that points that had at least one stressed season had more mortality (as measured in (Anderegg, Chegwidden, et al., 2022)) than points with zero stressed seasons (Figure 3). The distributions of mortality separated in this way were significantly different ($p \ll .001$) by both a Mann–Whitney *U* test (Mann & Whitney, 1947) and *t*-test (Yuen, 1974) as implemented in the Scipy package in Python (Virtanen et al., 2020) (see Table S2).

2.2.11 | Uncertainty analysis of future differences

We performed a bootstrap analysis to estimate the uncertainty in the difference of the 90th percentile PLC values (and 10th percentile leaf water potential values), as well as their differences. To perform the bootstrap analysis, we randomly selected 50% of the modeled days from the present, future, and both when doing a difference. We did this 100 times with replacement of days and calculated the 90th percentile each time for the present and future, as well as 100 times before calculating the difference between them. Uncertainty is reported as the 5–95th range of this ensemble of estimates. The 5–95th range is reported in Figure S10. Stippling was provided in Figures 1e–g and 5a,b where a difference had more than 5% of the distribution less than zero.

2.3 | Experimental setup

2.3.1 | Present-day runs 1995–2014

HOTTER experiments for the present day were run at a daily time step over the growing season (June, July, August) for the 20 years

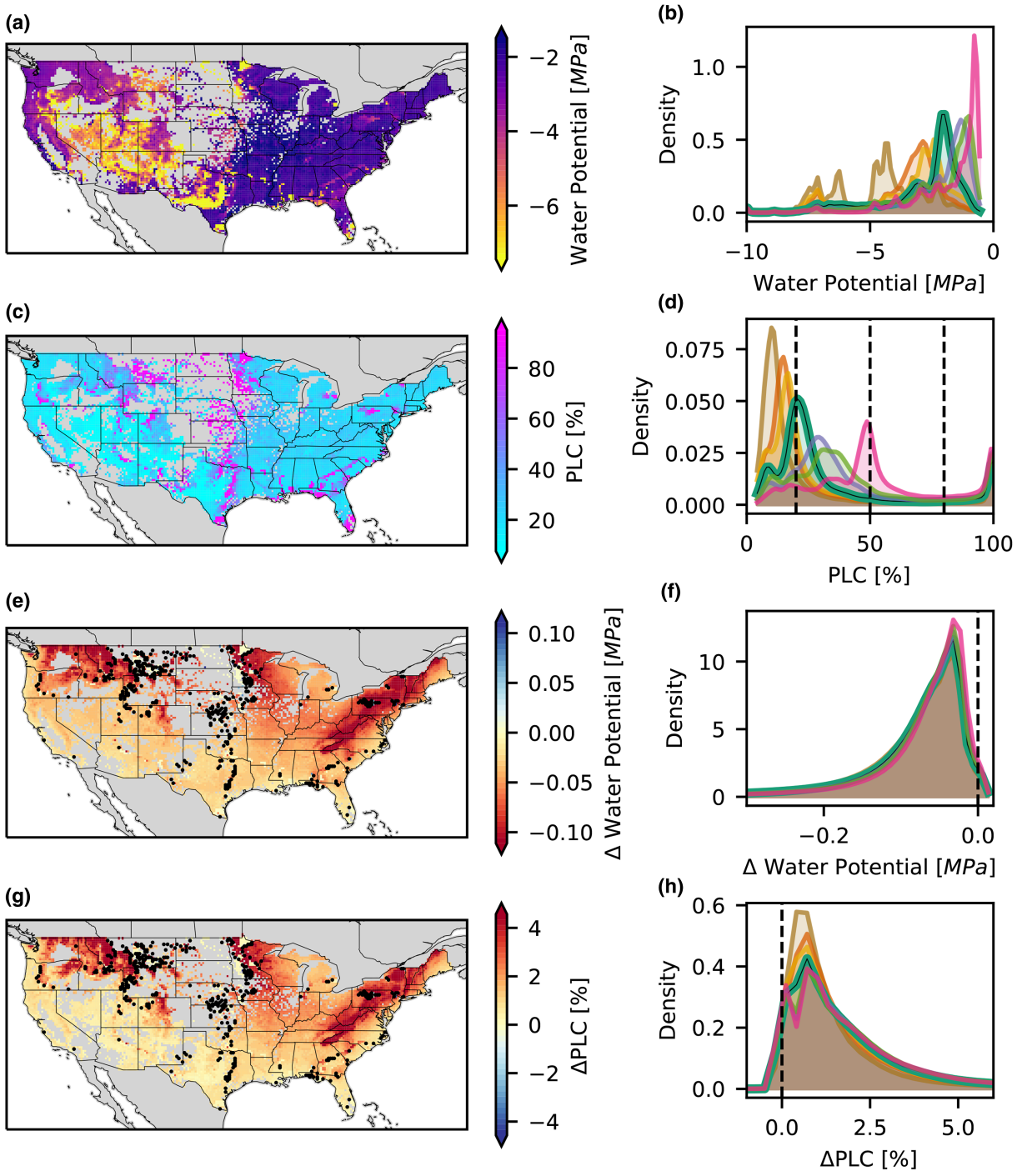

FIGURE 1 Climate change increases chronic hydraulic stress while geographic gradients in aridity and hydraulic traits mediate patterns of plant water status and stress. Model-predicted most stressed (10th percentile) daily leaf water potential (a) and most stressed (90th percentile) daily plant percent loss in conductivity (PLC) (c) calculated from 1995 to 2014 growing seasons. Change (future—historical) in the percentile of most stressed daily water potential (e) and the percentile of most stressed daily difference in PLC (g). Negative values in (e) indicate future decreases in plant water availability and positive values in (g) indicate future increases in stress. Maps show results for simulations parameterized with community mean hydraulic traits (CW mean). Histograms (b, d) include the 10% most stressed days, (f, h) include the difference between the 10% most stressed days in the present and those days in the future for each grid cell for hydraulic trait maps ranging from most drought vulnerable to least drought vulnerable species in a grid cell; "regional" corresponds with the most extreme trait values in a 0.25° grid cell, "plot" corresponds with average within-plot trait extremes, "CW" represents the min/mean/max community-weighted means across all forested plots in a grid cell. (e, g) Black stippling notes areas where the points are where the 5–95th percentile overlaps zero. Map lines delineate study areas and do not necessarily depict accepted national boundaries.

from 1995 to 2014 and across the continental United States at a resolution of 0.25 × 0.25 degrees latitude and longitude. The continental United States was chosen for the availability of daily estimates of soil water content and the mapped observations of P50 trait values. HOTTER forcings include temperature, vapor pressure deficit, soil water potential, height, and the average CO_2 for the period (370 ppm). In addition, the P50 values were taken from the mapped observations of P50 trait values. Seven separate experiments were done for each of the seven sets of P50 values (Figure S2; Table S3). For each experiment, tree leaf area is adaptively acclimated to maximize NPP for the entire 20-year simulation.

We ran sensitivity tests with different trait distributions used to parameterize the model, including community-weighted hydraulic traits weighted by species basal area within a forest plot, as well as the least and most vulnerable hydraulic traits co-located both within a plot and within a 0.25° climate grid cell (Figures S2 and S3). These sensitivity tests represent the range of scenarios where there may be shifts in plot composition toward species with more drought-resistant plant hydraulic traits or expansion of drought-resistant species to new stands within a region (i.e., a 0.25° climate grid cell where seed dispersal may be possible).

2.3.2 | Future runs 2081–2100

For the future runs, daily meteorology for temperature and vapor pressure deficit were created using the median values of the change in climate predicted by six models participating in CMIP6 for the "medium" SSP3-7.0 scenario that we chose to best match expectations for the trajectory of CO_2 emissions (see *Data Sources*). In addition to changing temperature and vapor pressure deficit, we applied a mean value of the change in atmospheric CO_2 concentrations (753 ppm). For these future experiments, we left the soil water potential unchanged from the present day as there is large uncertainty in soil water content change across models and the general prediction is that there will be relatively small changes (Mathias & Trugman, 2022). For future runs, we ran a number of different scenarios: with and without leaf acclimation, and attributing change to each of temperature, vapor pressure deficit, and atmospheric concentrations of CO_2. Collectively, these experiments enabled us to quantify the impact of individual future climate factors on forest stress and the extent to which adaptive acclimation in leaf area within a species may mitigate increased climate stress. See Table S3 for the experimental summary.

2.3.3 | Leaf acclimation

Future runs were performed using both the leaf area determined from the optimization in the present ("Fixed Leaf Area") and for leaf area that was optimized to maximize NPP over the future (2081–2100) period where temperature, vapor pressure deficit, and atmospheric concentrations of CO_2 change to expected future conditions consistent with the SSP 3-7.0 scenario in CMIP6 ("Acclimated Leaf Area") (Figure 4; Figures S8 and S12).

2.3.4 | Factorial runs

We quantified the effect of individual future climate factors, the adjustment of leaf area, and hydraulic trait diversity with a set of factorial experiments using the tree hydraulic model. We systematically included individual future forcings in isolation for the following climate factors combined with historical climate variables for the rest of the model forcing: VPD, atmospheric CO_2, and temperature (which impacted tree respiration and photosynthetic chemical reactions according to Mathias and Trugman (2022), but not VPD). We also tested the effect of adjustments in leaf area with experiments where leaf area remained optimized to historical conditions ("fixed leaf area") rather than being able to adjust to the future climate ("acclimated leaf area") (Figure S8).

2.4 | Software

The numerical modeling and analysis were performed in Python with the support of Anaconda installation with particularly heavy use of the following open-source modules: NumPy, Scipy, Xarray, Matplotlib, Cartopy (Hoyer & Hamman, 2017; Hunter, 2007; Met Office, 2010; van der Walt et al., 2011; Virtanen et al., 2020).

3 | RESULTS AND DISCUSSION

We first generated continental-scale maps of plant water status for the historical period for two widely used diagnostics of plant water status and water stress (respectively), leaf water potential, and percent loss in hydraulic conductivity (PLC). PLC characterizes the extent to which tree xylem transport vessels or tracheids are blocked by air bubbles formed by hydraulic stress which can be induced either by low water availability, high evaporative demand, or both (Venturas et al., 2017). Elevated PLC values have been linked to elevated tree mortality (Anderegg et al., 2015; Venturas et al., 2018). To capture the period of maximum stress in trees, we focus on days when leaf water potential was in the 10th percentile (e.g., the most negative leaf water potentials) and PLC was in the 90th percentile (e.g., PLC was highest) in each forested grid cell (see Material and Methods). We found that historical leaf water potential varied substantially across space due both to variations in aridity and hydraulic traits. The drier areas in the western United States had much more negative leaf water potentials, both because of drier soils and higher vapor pressure deficits (VPDs), and also because of the biogeographic ranges of more drought-tolerant tree populations that have more resistant hydraulic traits which allow trees to continue functioning at more negative water potentials without risking hydraulic damage (Figure 1a). Regions already experiencing elevated hydraulic

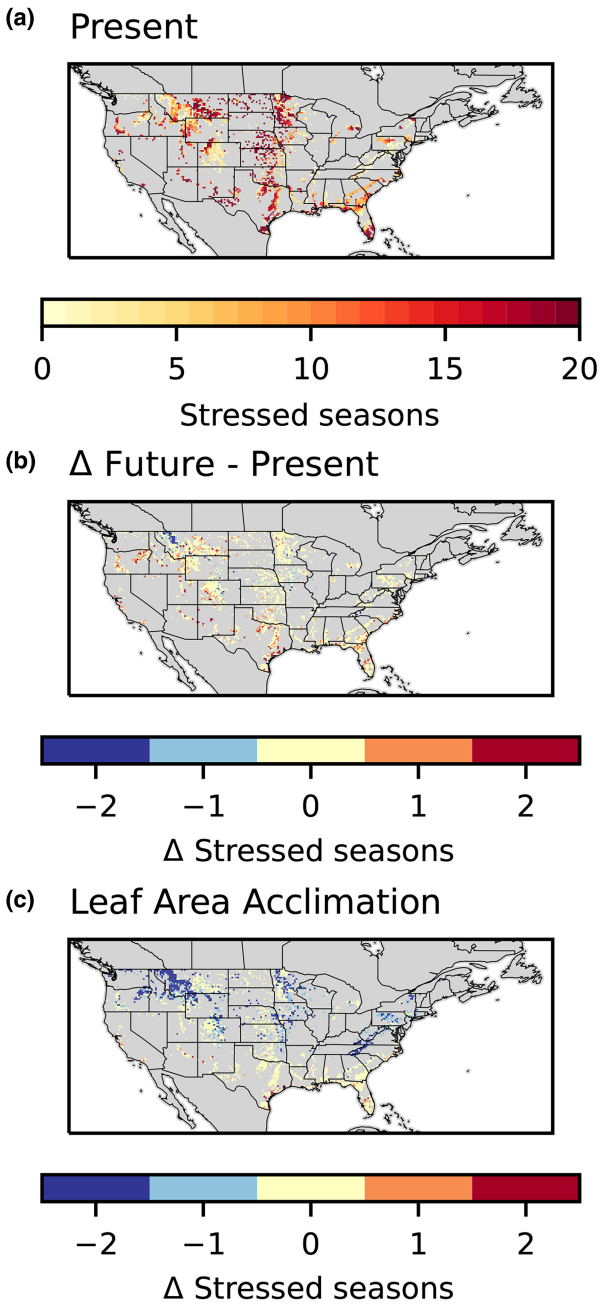

FIGURE 2 US forests are already experiencing growing seasons with potentially lethal levels of hydraulic stress, a trend which will likely continue with future climate change. The number of stressed historical growing seasons (a). Change in stressed growing seasons between historical and future climates with adaptive acclimation in tree leaf area (b) and difference (e.g., leaf acclimation effect) in the future with and without leaf area acclimation (c). Maps show results for simulations parameterized with community mean hydraulic traits. Gray coloration indicates no seasons with PLC >50%. For (a), redder colors indicate more seasons with PLC >50% with a maximum of 20 seasons over the 20-year historical simulation period. For (b, c), redder colors indicate an increase in the number of seasons with PLC >50% (e.g., an increase in potentially lethal stress), yellow indicates the same number of seasons with PLC >50% (e.g., no change in potentially lethal stress, but lethal stress predicted), blue indicates a decrease in seasons with PLC >50% or (b) between future climates with and without adaptive acclimation in leaf area. Map lines delineate study areas and do not necessarily depict accepted national boundaries.

stress in historical simulations included dry regions such as the US Mountain West where many species are resistant to water stress but climate change has increased drought frequency and severity (Diffenbaugh et al., 2015; Marvel et al., 2021). Despite wetter baseline conditions, parts of the Midwest and eastern United States also saw elevated PLCs because of more hydraulically vulnerable trait compositions (Figure 1c). This may be due in part to microsite variations in water availability that are not captured by our climate forcing, resulting in overprediction of stress in some midwestern areas where forest cover is sparse and restricted to riparian areas. Also, note that parts of the Midwest that show large stress in the present day are also some of the most uncertain regions (Figure S10).

With projected increases in temperatures and VPDs circa 2081–2100 for an intermediate climate change scenario (shared socio-economic pathway (SSP) 3-7.0 emissions scenario), we found increases in the 90th percentile of daily PLC, indicating systematic increases in chronic stress throughout the United States (Figure 1e,g). However, with leaf area acclimation, the northeastern United States showed reduced chronic stress due to tree model adjustments to lower leaf area associated with warmer temperatures (Figures S7–S10). In regions of the South and Mountain West, the systematic increases in stress are occurring under novel combinations of temperature and VPD not represented in the present-day climate (Figure S11). Such novel climates make it particularly important to understand the fundamental mechanistic trade-offs that trees face with increasing climate stress. Interestingly, warmer future temperatures increased the respiratory cost of leaves relative to their carbon gain potential, reducing leaf area enough to ameliorate hydraulic stress (Materials and Methods). Depending on species' drought vulnerability, some increases in PLC were mediated by more drought-resistant traits either within local forest plots or the regional climate grid cell (Figure 1b,d,f,h). However, locations throughout the Mountain West, Midwest, and Southeast were found to be already experiencing potentially lethal levels of stress (Figures 1c and 2a). Climate stress in these regions is expected to accelerate under future climates (Figures 1e–g and 2b,c), a pattern that has been documented in numerous observational studies of widespread tree mortality (Anderegg et al., 2012; Anderegg, Wu, et al., 2022; Breshears et al., 2005, p. 20015; Hammond et al., 2022; Figure 3a–d).

Model-predicted hydraulic stress, either through elevated PLC or stressed seasons, corresponded well with forest inventory-observed elevated mortality (Figure 3a–d). While tree mortality has proven difficult to predict, we find that high values of present-day PLC or stressed seasons in the model relate to higher levels of observed mortality and offered substantial improvements over standard drought metrics such as SPEI (Figure 3e,f; Kolb, 2015; Mathias & Trugman, 2022; Venturas et al., 2021). Specifically, we find significantly elevated rates of mortality at grid points where the 90th percentile of daily PLC is greater than 25% or where there has been

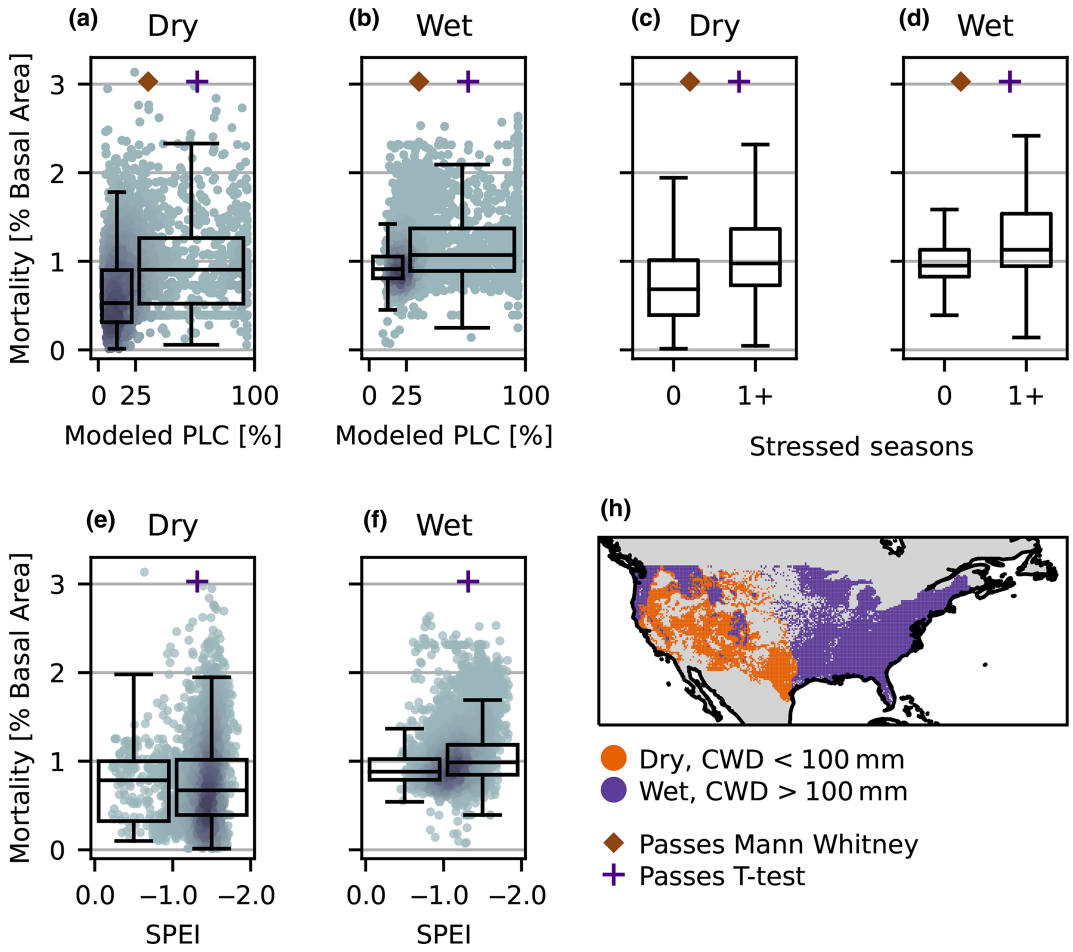

FIGURE 3 The plant hydraulic model substantially increases predictive skill for drought mortality compared to standard drought metrics in both dry and wet climates across United States. Comparison of the mortality with 90th percentile of daily PLC modeled for the present for unstressed (PLC <25%) or stressed (PLC >25%) for (a) dry regions, (b) wet regions. Comparison mortality and the occurrence of a stressed season for (c) dry regions and (d) wet regions. Comparison of mortality and the driest 10% of SPEI drought index for the growing season in (e) dry regions and (f) wet regions. (g) Dry and wet regions of the United States determined by climate water deficit. Mortality is measured as the distribution of the percent basal area mortality observed in the US Forest inventory for climate grid cells. For (a, b, e, f), the point shading represents the density of points. For (a–f), center line, median; box limits, upper and lower quartiles; whiskers, 1.5× interquartile range. (a–f) If distributions represented by boxplots pass the Mann–Whitney test plot brown diamond or *t*-test (purple plus), see Table S2.

at least one stressed season in the study period—this is true for both dry and wet regions (Figure 3a–d). In addition, we find no significant difference or a negative response (less mortality with stronger drought) when dividing the mortality observations with the SPEI drought index (Figure 3e,f; Vicente-Serrano et al., 2010). The ability of the physiologically based model using observed hydraulic traits to identify points with a higher risk of mortality supports the utility of the model in predicting change in plant hydraulic stress beyond climate alone (as represented by the SPEI drought index).

Model projections indicate that most of the stressed daily PLC values will increase by ~1–2% with future climate change. While this increase in PLC appears small in comparison to the measurement precision of current hydraulic techniques (Venturas et al., 2017), this across-the-board increase in chronic stress is concerning for long-term forest health because it represents a shift in baseline stress conditions during times of already high stress (related to tree mortality (Figure 3)), which feedback to further decrease plant health through "cavitation fatigue" (Hacke et al., 2001), or legacy effects on growth (Anderegg et al., 2015). Our results show that the majority of US forests may face elevated chronic stress moving forward that will be compounded when trees experience expected increases in acute stress due to higher frequency droughts associated with novel climate extremes (Diffenbaugh et al., 2015). This means that even drought-resistant species may become more vulnerable to drought events over time due to chronic mechanical stress in hydraulic tissues that results in higher conductivity losses at less negative water potentials (e.g., at higher water availability) for the same tree due to cavitation fatigue (Hacke et al., 2001).

Projected stress effects varied by region due to the wide climate and trait gradients across the United States. We compared the effects of future climate factors, traits, and leaf acclimation in the diverse regions of the cool and wet Pacific Northwest (PNW) with projected more moderate changes in temperature and VPD, the cool and wet Northeast (NE) with projected larger changes in

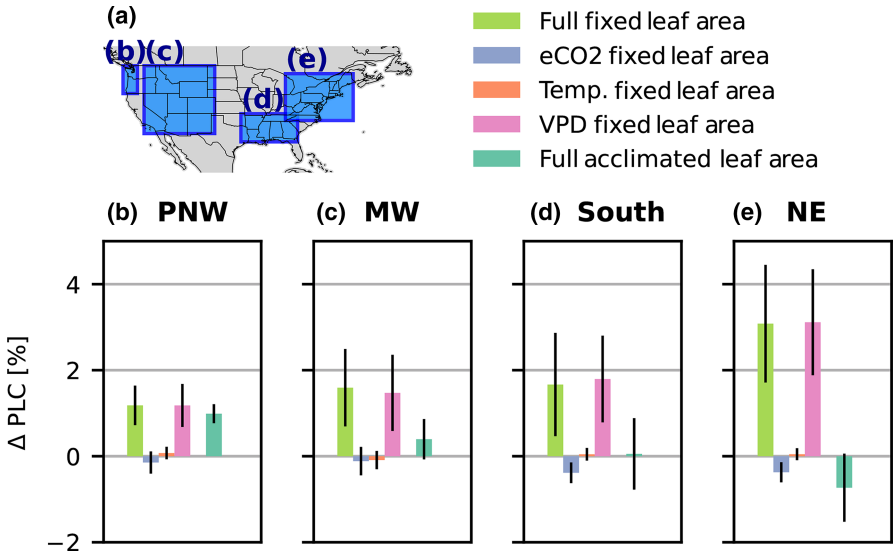

FIGURE 4 Projected stress effects of climate change on forests varies by region due to large gradients in aridity and traits across the continental United States. Regional (shown in panel a in blue) changes in the most stressed 10% of the daily percent loss of conductivity for the Pacific Northwest (PNW) (b), North East (NE) (c), Mountain West (MW) (d), and South East (e). Individual bars show changes attributed to the full combined climate change effect (Full), future vapor pressure deficits (VPD), temperature (Temp), and CO_2 (eCO_2) with fixed leaf area and the full combined effect with adaptive acclimation of leaf area to maximize carbon gain. Values are for the community-weighted (CW) P50 map, the rest of the permutations in trait values are shown in Figure S12. Map lines delineate study areas and do not necessarily depict accepted national boundaries.

temperature and VPD (Figure S7), the hot and dry Mountain west (MW), and the hot and wet South (Figure 4; Figure S12). Across all locations, all else equal, elevated CO_2 levels had an ameliorating effect on water stress due to increased water use efficiency (Walker et al., 2021). Projected increases in VPD increased stress across all regions, though the magnitude of this effect varied widely depending on the region. Temperature change did not have a large effect with fixed leaf area. We also found that both traits and adjustment in leaf area had the potential to alter future forest stress. In particular and depending on location, adjustment in leaf area to maximize carbon gain could reduce the increase in the 90th percentile of PLC between historical and future by >5.4%, even reversing the sign so that some locations saw a decrease in stress with future climate. Note that leaf area acclimation had little impact on stress in the Pacific northwest, while the stress reversal effect occurred in locations where high temperature drove declines in leaf area—particularly the NE. Potential range expansions of drought-resistant species within a grid cell that changed community hydraulic trait values also ameliorated PLC stress, though the effect was more moderate (>2.1%, between the least and most drought vulnerable traits at a grid point).

We calculated the extent to which biogeographic shifts and changes in community trait composition are required to avoid projected future increases in chronic (90th percentile daily PLC) stress and compared these values to observed shifts in community-weighted traits (i.e., trait velocities or the change in community-weighted trait values over time) derived from the US Forest Inventory and Analysis database. We found that across the United States, almost all locations required some shift in forest hydraulic traits to avoid increased stress (Figure 5). In instances where leaf area adjustment was not possible, 72.5% of forested grid cells required a shift in composition comparable to the community mean of the most drought-resistant forest plot within the grid cell (51.7% with leaf area adjustment) (Figure 5a,b). Furthermore, 12.3% (10.0% with leaf area adjustment) of grid cells did not have sufficiently drought-resistant traits to mitigate increases in stress. Finally, only 2.2% of cells (33.6% with leaf area adjustment) required no shift in composition whatsoever to avoid future climate stress. Although we found substantial overlap in the distributions of the observed trait velocities and model-required trait velocities to maintain historical levels of PLC stress, mean velocities required to maintain historical stress were an order of magnitude higher than what was quantified from the observations based on forest inventory data (−0.0143 MPa $year^{-1}$ needed without leaf area acclimation vs. −0.0022 MPa $year^{-1}$ observed) (Trugman et al., 2020) and 81% of grid cells had observed trait shifts that were slower than required in the model to avoid increased stress (47% with leaf area acclimation). The mismatch between required and observed trait velocities indicates that current shifts in forest trait composition are not sufficient to avoid increased hydraulic stress from climate change.

The size of the effect of leaf area allocation on our projections of stress in the future highlights the power of acclimation for forests under future conditions. However, carbon allocation strategies under future climate conditions and increased atmospheric CO_2 remain uncertain (De Kauwe et al., 2014). While we assume that carbon will be allocated to leaves to maximize carbon gain in this study—the tree balances water stress with carbon gain through its impact on photosynthesis—it is possible that trees will instead allocate carbon for other reasons (e.g., competition for water and light

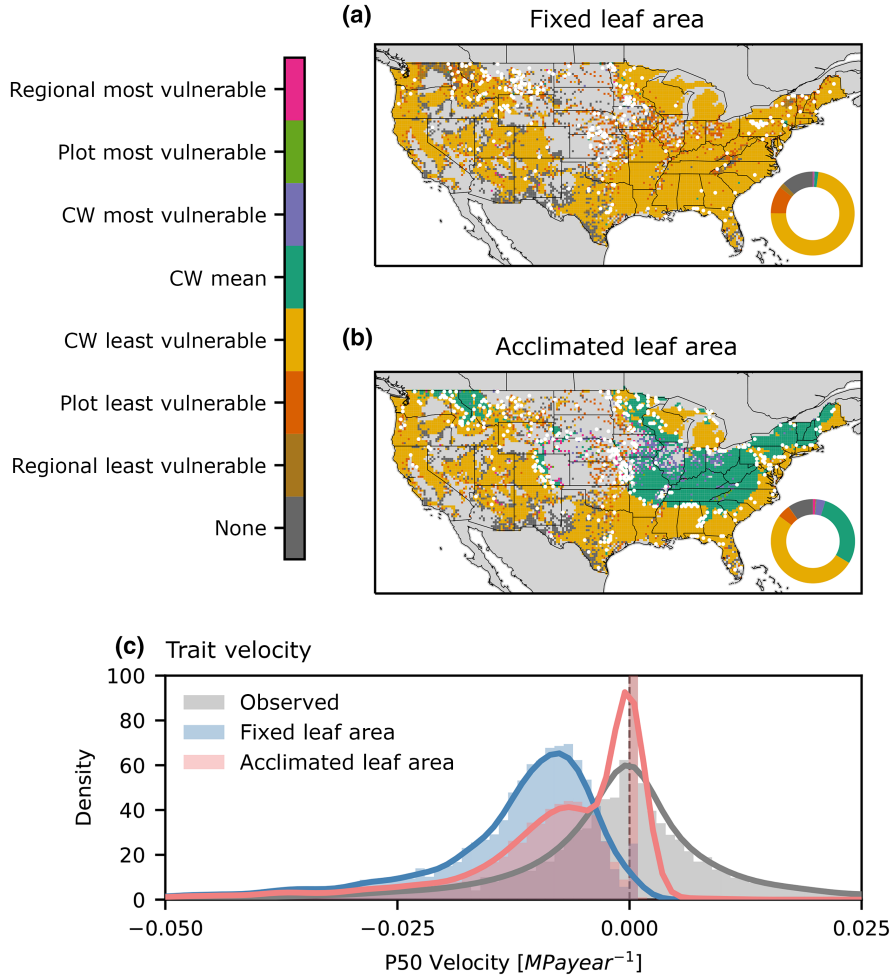

FIGURE 5 Species range shifts could buffer against future climate-induced hydraulic stress in a majority of locations, but observed trait velocities are not currently keeping pace with the required compositional shifts to mitigate increases in stress. Shift in P50 under future climates relative to current community mean P50 required to avoid increased hydraulic, without (a) and with (b) adaptive leaf area acclimation in future climates. Gold, orange, and brown indicate at least some shift toward more drought-resistant (more negative) P50s is required to avoid increased chronic daily stress. Dark gray values are areas where no P50 values within the region are sufficient to avoid increased hydraulic stress. Turquoise indicates that no shift in P50 is required to avoid increases in stress. Purple, green, and pink indicate that shifts toward more drought vulnerable P50 values (less negative) are possible without increasing stress. Circles indicate the relative abundance of grid cells associated with each color. (c) The distribution of P50 velocities observed (gray) from the US Forest Inventory across the continental United States compared to model required values in (a, b) for predictions with a fixed leaf area (blue) and acclimated leaf area (red). (a, b) White stippling notes areas where the points are where the 5–95th percentile overlaps zero. Map lines delineate study areas and do not necessarily depict accepted national boundaries.

[Farrior et al., 2013]). The ability to avoid some future stress through acclimation highlights the need to incorporate leaf area allocation strategies in response to plant water stress in prognostic terrestrial biosphere models along with the demographic changes in the ecosystem (Fisher et al., 2015; Trugman, Anderegg, Wolfe, et al., 2019).

Predicting biogeographic transitions in forest species across climate gradients from first principles has been an unsolved problem in the ecological and vegetation modeling communities for over a decade (Fisher et al., 2015). Here, we use a hydraulically enabled vegetation model parameterized with a hydraulic trait database and high-resolution surveys of species distribution and abundance to diagnose current and future projected climate stress of US forests. We find that climate change will likely increase chronic water stress in US forest, potentially resulting in shifts in the composition and biogeography of forests toward more drought-tolerant trees, even with within-species leaf area acclimation. Without shifts in forest composition or acclimation, increased water stress may accelerate tree mortality, offsetting potential carbon sink gains from CO_2 fertilization.

AUTHOR CONTRIBUTIONS

G. R. Quetin and A. T. Trugman designed the study with input from L. D. L. Anderegg, I. Boving, and W. R. L. Anderegg. G. R. Quetin updated the tree hydraulic model and performed the analysis. G. R. Quetin and A. T. Trugman wrote the paper with all authors contributing comments.

ACKNOWLEDGMENTS

This research was funded by NSF Grant 2003205. ATT acknowledges funding from the NSF Grants 2017949 and 2216855, the USDA National Institute of Food and Agriculture, Agricultural and Food Research Initiative Competitive Programme Grant No. 2018-67012-31496.

CONFLICT OF INTEREST STATEMENT

None.

DATA AVAILABILITY STATEMENT

The analysis code supporting this publication is available online at 10.6084/m9.figshare.21643949. The model code supporting this publication is available online at 10.6084/m9.figshare.21644192. The data that support the findings of this study are publicly available online at 10.6084/m9.figshare.21642332. All other datasets used in this analysis are publicly available.

ORCID

G. R. Quetin https://orcid.org/0000-0002-7884-5332
L. D. L. Anderegg https://orcid.org/0000-0002-5144-7254
W. R. L. Anderegg https://orcid.org/0000-0001-6551-3331
A. T. Trugman https://orcid.org/0000-0002-7903-9711

REFERENCES

Abatzoglou, J. T., Dobrowski, S. Z., Parks, S. A., & Hegewisch, K. C. (2018). TerraClimate, a high-resolution global dataset of monthly climate and climatic water balance from 1958–2015. *Scientific Data*, *5*(1), 170191. https://doi.org/10.1038/sdata.2017.191

Adams, H. D., Macalady, A. K., Breshears, D. D., Allen, C. D., Stephenson, N. L., Saleska, S. R., Huxman, T. E., & McDowell, N. (2010). Climate-induced tree mortality: Earth system consequences. *Eos, Transactions American Geophysical Union*, *91*(17), 153–154.

Allen, C. D., & Breshears, D. D. (1998). Drought-induced shift of a forest–woodland ecotone: Rapid landscape response to climate variation. *Proceedings of the National Academy of Sciences*, *95*(25), 14839–14842.

Anderegg, L. D., Griffith, D. M., Cavender-Bares, J., Riley, W. J., Berry, J. A., Dawson, T. E., & Still, C. J. (2022). Representing plant diversity in land models: An evolutionary approach to make "functional types" more functional. *Global Change Biology*, *28*(8), 2541–2554.

Anderegg, W. R. L., Chegwidden, O., Badgley, G., Trugman, A. T., Cullenward, D., Abatzoglou, J. T., Hicke, J. A., Freeman, J., & Hamman, J. J. (2022). Future climate risks from stress, insects, and fire across US forests. *Ecology Letters*, *25*(6), 1510–1520.

Anderegg, L. D., & HilleRisLambers, J. (2019). Local range boundaries vs. large-scale trade-offs: Climatic and competitive constraints on tree growth. *Ecology Letters*, *22*(5), 787–796.

Anderegg, L. D., Loy, X., Markham, I. P., Elmer, C. M., Hovenden, M. J., HilleRisLambers, J., & Mayfield, M. M. (2021). Aridity drives coordinated trait shifts but not decreased trait variance across the geographic range of eight Australian trees. *New Phytologist*, *229*(3), 1375–1387.

Anderegg, W. R., Schwalm, C., Biondi, F., Camarero, J. J., Koch, G., Litvak, M., Ogle, K., Shaw, J. D., Shevliakova, E., Williams, A. P., Wolf, A., Ziaco, E., & Pacala, S. (2015). Pervasive drought legacies in forest ecosystems and their implications for carbon cycle models. *Science*, *349*(6247), 528–532.

Anderegg, W. R. L., Berry, J. A., Smith, D. D., Sperry, J. S., Anderegg, L. D. L., & Field, C. B. (2012). The roles of hydraulic and carbon stress in a widespread climate-induced forest die-off. *Proceedings of the National Academy of Sciences*, *109*(1), 233–237. https://doi.org/10.1073/pnas.1107891109

Anderegg, W. R. L., Wolf, A., Arango-Velez, A., Choat, B., Chmura, D. J., Jansen, S., Kolb, T., Li, S., Meinzer, F. C., Pita, P., Resco de Dios, V., Sperry, J. S., Wolfe, B. T., & Pacala, S. (2018). Woody plants optimise stomatal behaviour relative to hydraulic risk. *Ecology Letters*, *21*(7), 968–977. https://doi.org/10.1111/ele.12962

Anderegg, W. R. L., Wu, C., Acil, N., Carvalhais, N., Pugh, T. A. M., Sadler, J. P., & Seidl, R. (2022). A climate risk analysis of Earth's forests in the 21st century. *Science*, *377*(6610), 1099–1103. https://doi.org/10.1126/science.abp9723

Barton, C. V., & Montagu, K. D. (2006). Effect of spacing and water availability on root: Shoot ratio in Eucalyptus camaldulensis. *Forest Ecology and Management*, *221*(1–3), 52–62.

Bonan, G. B. (2002). *Ecological climatology: Concepts and applications*. Cambridge University Press.

Breshears, D. D., Cobb, N. S., Rich, P. M., Price, K. P., Allen, C. D., Balice, R. G., Romme, W. H., Kastens, J. H., Floyd, M. L., Belnap, J., Anderson, J. J., Myers, O. B., & Meyer, C. W. (2005). Regional vegetation die-off in response to global-change-type drought. *Proceedings of the National Academy of Sciences*, *102*(42), 15144–15148. https://doi.org/10.1073/pnas.0505734102

Campbell, G. S. (1974). A simple method for determining unsaturated conductivity from moisture retention data. *Soil Science*, *117*(6) Retrieved from https://journals.lww.com/soilsci/Fulltext/1974/06000/A_SIMPLE_METHOD_FOR_DETERMINING_UNSATURATED.1.aspx, 311–314.

Cano, I. M., Shevliakova, E., Malyshev, S., John, J. G., Yu, Y., Smith, B., & Pacala, S. W. (2022). Abrupt loss and uncertain recovery from fires of Amazon forests under low climate mitigation scenarios. *Proceedings of the National Academy of Sciences*, *119*(52), e2203200119. https://doi.org/10.1073/pnas.2203200119

Chen, I.-C., Hill, J. K., Ohlemüller, R., Roy, D. B., & Thomas, C. D. (2011). Rapid range shifts of species associated with high levels of climate warming. *Science*, *333*(6045), 1024–1026. https://doi.org/10.1126/science.1206432

Colwell, R. K., Brehm, G., Cardelús, C. L., Gilman, A. C., & Longino, J. T. (2008). Global warming, elevational range shifts, and lowland biotic attrition in the wet tropics. *Science*, *322*(5899), 258–261. https://doi.org/10.1126/science.1162547

Cox, P. M., Betts, R. A., Jones, C. D., Spall, S. A., & Totterdell, I. J. (2000). Acceleration of global warming due to carbon-cycle feedbacks in a coupled climate model. *Nature*, *408*(6813), 750.

De Kauwe, M. G., Medlyn, B. E., Zaehle, S., Walker, A. P., Dietze, M. C., Wang, Y. P., Luo, Y., Jain, A. K., El-Masri, B., Hickler, T., Wårlind, D., Weng, E., Parton, W. J., Thornton, P. E., Wang, S., Prentice, I. C., Asao, S., Smith, B., McCarthy, H. R., … Norby, R. J. (2014). Where does the carbon go? A model–data intercomparison of vegetation carbon allocation and turnover processes at two temperate forest free-air CO_2 enrichment sites. *New Phytologist*, *203*, 883–899.

Diffenbaugh, N. S., Swain, D. L., & Touma, D. (2015). Anthropogenic warming has increased drought risk in California. *Proceedings of the National Academy of Sciences*, *112*(13), 3931–3936.

Eller, C. B., de Barros, F. V., Bittencourt, R. L., Rowland, P., Mencuccini, M. L., & Oliveira, S. R. (2018). Xylem hydraulic safety and construction costs determine tropical tree growth: Tree growth vs hydraulic safety trade-off. *Plant, Cell & Environment*, *41*(3), 548–562. https://doi.org/10.1111/pce.13106

Esquivel-Muelbert, A., Baker, T. R., Dexter, K. G., Lewis, S. L., Brienen, R. J. W., Feldpausch, T. R., Lloyd, J., Monteagudo-Mendoza, A., Arroyo, L., Álvarez-Dávila, E., Higuchi, N., Marimon, B. S., Marimon-Junior, B. H., Silveira, M., Vilanova, E., Gloor, E., Malhi, Y., Chave,

J., Barlow, J., … Phillips, O. L. (2019). Compositional response of Amazon forests to climate change. *Global Change Biology*, *25*(1), 39–56. https://doi.org/10.1111/gcb.14413

Eyring, V., Bony, S., Meehl, G. A., Senior, C. A., Stevens, B., Stouffer, R. J., & Taylor, K. E. (2016). Overview of the coupled model intercomparison project phase 6 (CMIP6) experimental design and organization. *Geoscientific Model Development*, *9*(5), 1937–1958.

Farrior, C. E., Dybzinski, R., Levin, S. A., & Pacala, S. W. (2013). Competition for water and light in closed-canopy forests: A tractable model of carbon allocation with implications for carbon sinks. *The American Naturalist*, *181*(3), 314–330.

Fisher, R. A., Muszala, S., Verteinstein, M., Lawrence, P., Xu, C., McDowell, N. G., Knox, R. G., Koven, C., Holm, J., Rogers, B. M., Spessa, A., Lawrence, D., & Bonan, G. (2015). Taking off the training wheels: The properties of a dynamic vegetation model without climate envelopes, CLM4. 5 (ED). *Geoscientific Model Development*, *8*(11), 3593–3619.

García-Valdés, R., Vayreda, J., Retana, J., & Martínez-Vilalta, J. (2021). Low forest productivity associated with increasing drought-tolerant species is compensated by an increase in drought-tolerance richness. *Global Change Biology*, *27*(10), 2113–2127.

Hacke, U. G., Sperry, J. S., Pockman, W. T., Davis, S. D., & McCulloh, K. A. (2001). Trends in wood density and structure are linked to prevention of xylem implosion by negative pressure. *Oecologia*, *126*(4), 457–461. https://doi.org/10.1007/s004420100628

Hammond, W. M., Williams, A. P., Abatzoglou, J. T., Adams, H. D., Klein, T., López, R., Sáenz-Romero, C., Hartmann, H., Breshears, D. D., & Allen, C. D. (2022). Global field observations of tree die-off reveal hotter-drought fingerprint for Earth's forests. *Nature Communications*, *13*(1), 1761. https://doi.org/10.1038/s41467-022-29289-2

Hoyer, S., & Hamman, J. (2017). Xarray: nd labeled arrays and datasets in Python. *Journal of Open Research Software*, *5*(1), 10. https://doi.org/10.5334/jors.148

Hunter, J. D. (2007). Matplotlib: A 2D graphics environment. *Computing in Science & Engineering*, *9*(3), 90–95. https://doi.org/10.1109/MCSE.2007.55

Keeling, R., Piper, S., Bollenbacher, A., & Walker, J. (2009). *Atmospheric Carbon Dioxide Record from Mauna Loa* (1958-2008). Carbon Dioxide Information Analysis Center (CDIAC), Oak Ridge National. Retrieved from www.esrl.noaa.gov/gmd/ccgg/trends/

Keeling, R. F., Graven, H. D., Welp, L. R., Resplandy, L., Bi, J., Piper, S. C., Sun, Y., Bollenbacher, A., & Meijer, H. A. J. (2017). Atmospheric evidence for a global secular increase in carbon isotopic discrimination of land photosynthesis. *Proceedings of the National Academy of Sciences*, *114*(39), 10361–10366. https://doi.org/10.1073/pnas.1619240114

Kolb, T. E. (2015). A new drought tipping point for conifer mortality. *Environmental Research Letters*, *10*(3), 031002. https://doi.org/10.1088/1748-9326/10/3/031002

Kurz, W. A., Dymond, C. C., Stinson, G., Rampley, G. J., Neilson, E. T., Carroll, A. L., Ebata, T., & Safranyik, L. (2008). Mountain pine beetle and forest carbon feedback to climate change. *Nature*, *452*(7190), 987–990.

Lenoir, J., Gégout, J. C., Marquet, P. A., de Ruffray, P., & Brisse, H. (2008). A significant upward shift in plant species optimum elevation during the 20th century. *Science*, *320*(5884), 1768–1771. https://doi.org/10.1126/science.1156831

Li, B., Beaudoing, H., & Rodell, M. (2020). *GLDAS Catchment Land Surface Model L4 daily 0.25 × 0.25 degree GRACE-DA1 V2. 2*. Greenbelt, Maryland, USA, Goddard Earth Sciences Data and Information Services Center (GES DISC) Goddard Earth Sci Data Inf Serv Cent (GES DISC), *16*(1), 1–32. https://doi.org/10.5067/TXBMLX370XX8

Li, B., Rodell, M., Kumar, S., Beaudoing, H. K., Getirana, A., Zaitchik, B. F., Goncalves, L. G., Cossetin, C., Bhanja, S., Mukherjee, A., Tian, S., Tangdamrongsub, N., Long, D., Nanteza, J., Lee, J., Policelli, F., Goni, I. B., Daira, D., Bila, M., … Bettadpur, S. (2019). Global GRACE data assimilation for groundwater and drought monitoring: Advances and challenges. *Water Resources Research*, *55*(9), 7564–7586. https://doi.org/10.1029/2018WR024618

Liu, A., Cheng, X., & Chen, Z. (2021). Performance evaluation of GEDI and ICESat-2 laser altimeter data for terrain and canopy height retrievals. *Remote Sensing of Environment*, *264*, 112571. https://doi.org/10.1016/j.rse.2021.112571

Liu, H., Ye, Q., Gleason, S. M., He, P., & Yin, D. (2021). Weak tradeoff between xylem hydraulic efficiency and safety: Climatic seasonality matters. *New Phytologist*, *229*(3), 1440–1452. https://doi.org/10.1111/nph.16940

Louthan, A. M., Doak, D. F., & Angert, A. L. (2015). Where and when do species interactions set range limits? *Trends in Ecology & Evolution*, *30*(12), 780–792.

MacArthur, R. H. (1984). *Geographical ecology: Patterns in the distribution of species*. Princeton University Press.

Machado, R., Loram-Lourenço, L., Farnese, F. S., Alves, R. D. F. B., de Sousa, L. F., Silva, F. G., Filho, S. C. V., Torres-Ruiz, J. M., Cochard, H., & Menezes-Silva, P. E. (2021). Where do leaf water leaks come from? Trade-offs underlying the variability in minimum conductance across tropical savanna species with contrasting growth strategies. *New Phytologist*, *229*(3), 1415–1430.

Mackay, D. S., Savoy, P. R., Grossiord, C., Tai, X., Pleban, J. R., Wang, D. R., McDowell, N. G., Adams, H. D., & Sperry, J. S. (2020). Conifers depend on established roots during drought: Results from a coupled model of carbon allocation and hydraulics. *New Phytologist*, *225*(2), 679–692.

Mann, H. B., & Whitney, D. R. (1947). On a test of whether one of two random variables is stochastically larger than the other. *The Annals of Mathematical Statistics*, *18*, 50–60.

Martínez-Vilalta, J., Cochard, H., Mencuccini, M., Sterck, F., Herrero, A., Korhonen, J. F. J., Llorens, P., Nikinmaa, E., Nolè, A., Poyatos, R., Ripullone, F., Sass-Klaassen, U., & Zweifel, R. (2009). Hydraulic adjustment of scots pine across Europe. *New Phytologist*, *184*(2), 353–364.

Marvel, K., Cook, B. I., Bonfils, C., Smerdon, J. E., Williams, A. P., & Liu, H. (2021). Projected changes to hydroclimate seasonality in the continental United States. *Earth'sFutures*, *9*(9), e2021EF002019.

Mathias, J. M., & Trugman, A. T. (2022). Climate change impacts plant carbon balance, increasing mean future carbon use efficiency but decreasing total forest extent at dry range edges. *Ecology Letters*, *25*(2), 498–508. https://doi.org/10.1111/ele.13945

Mencuccini, M., & Grace, J. (1995). Climate influences the leaf area/sapwood area ratio in scots pine. *Tree Physiology*, *15*(1), 1–10.

Met Office, U. (2010). Cartopy: A cartographic Python library with a matplotlib interface. Exeter

Navarro-Racines, C., Tarapues, J., Thornton, P., Jarvis, A., & Ramirez-Villegas, J. (2020). High-resolution and bias-corrected CMIP5 projections for climate change impact assessments. *Scientific Data*, *7*(1), 1–14.

O'Neill, B. C., Tebaldi, C., Van Vuuren, D. P., Eyring, V., Friedlingstein, P., Hurtt, G., Knutti, R., Kriegler, E., Lamarque, J.-F., Lowe, J., Meehl, G. A., Moss, R., Riahi, K., & Sanderson, B. M. (2016). The scenario model intercomparison project (ScenarioMIP) for CMIP6. *Geoscientific Model Development*, *9*(9), 3461–3482.

Park Williams, A., Allen, C. D., Macalady, A. K., Griffin, D., Woodhouse, C. A., Meko, D. M., Swetnam, T. W., Rauscher, S. A., Seager, R., Grissino-Mayer, H. D., Dean, J. S., Cook, E. R., Gangodagamage, C., Cai, M., & McDowell, N. G. (2013). Temperature as a potent driver of regional forest drought stress and tree mortality. *Nature Climate Change*, *3*(3), 292–297.

Peters, M. P., Iverson, L. R., & Matthews, S. N. (2015). Long-term drought-tiness and drought tolerance of eastern US forests over five decades. *Forest Ecology and Management*, *345*, 56–64.

Piñol, J., & Sala, A. (2000). Ecological implications of xylem cavitation for several Pinaceae in the Pacific Northern USA. *Functional Ecology*, *14*(5), 538–545.

Potapov, P., Li, X., Hernandez-Serna, A., Tyukavina, A., Hansen, M. C., Kommareddy, A., Pickens, A., Turubanova, S., Tang, H., Silva, C. E., Armston, J., Dubayah, R., Blair, J. B., & Hofton, M. (2021). Mapping global forest canopy height through integration of GEDI and Landsat data. *Remote Sensing of Environment*, *253*, 112165. https://doi.org/10.1016/j.rse.2020.112165

Rosas, T., Mencuccini, M., Barba, J., Cochard, H., Saura-Mas, S., & Martínez-Vilalta, J. (2019). Adjustments and coordination of hydraulic, leaf and stem traits along a water availability gradient. *New Phytologist*, *223*(2), 632–646.

Sabot, M. E. B., Kauwe, M. G., Pitman, A. J., Medlyn, B. E., Ellsworth, D. S., Martin-StPaul, N. K., Wu, J., Choat, B., Limousin, J., Mitchell, P. J., Rogers, A., & Serbin, S. P. (2022). One stomatal model to rule them all? Towards improved representation of carbon and water exchange in global models. *Journal of Advances in Modeling Earth Systems*, *14*. https://doi.org/10.1029/2021MS002761

Seidl, R., & Turner, M. G. (2022). Post-disturbance reorganization of forest ecosystems in a changing world. *Proceedings of the National Academy of Sciences*, *119*(28), e2202190119.

Smith, N. G., Keenan, T. F., Colin Prentice, I., Wang, H., Wright, I. J., Niinemets, Ü., Crous, K. Y., Domingues, T. F., Guerrieri, R., Yoko Ishida, F., Kattge, J., Kruger, E. L., Maire, V., Rogers, A., Serbin, S. P., Tarvainen, L., Togashi, H. F., Townsend, P. A., Wang, M., … Zhou, S. X. (2019). Global photosynthetic capacity is optimized to the environment. *Ecology Letters*, *22*, 506–517. https://doi.org/10.1111/ele.13210

Sperry, J. S., Venturas, M. D., Anderegg, W. R. L., Mencuccini, M., Mackay, D. S., Wang, Y., & Love, D. M. (2017). Predicting stomatal responses to the environment from the optimization of photosynthetic gain and hydraulic cost: A stomatal optimization model. *Plant, Cell & Environment*, *40*(6), 816–830. https://doi.org/10.1111/pce.12852

Sperry, J. S., Wang, Y., Wolfe, B. T., Mackay, D. S., Anderegg, W. R. L., McDowell, N. G., & Pockman, W. T. (2016). Pragmatic hydraulic theory predicts stomatal responses to climatic water deficits. *New Phytologist*, *212*(3), 577–589. https://doi.org/10.1111/nph.14059

Trugman, A. T., Anderegg, L. D. L., Shaw, J. D., & Anderegg, W. R. L. (2020). Trait velocities reveal that mortality has driven widespread coordinated shifts in forest hydraulic trait composition. *Proceedings of the National Academy of Sciences*, *117*(15), 8532–8538. https://doi.org/10.1073/pnas.1917521117

Trugman, A. T., Anderegg, L. D. L., Sperry, J. S., Wang, Y., Venturas, M., & Anderegg, W. R. L. (2019). Leveraging plant hydraulics to yield predictive and dynamic plant leaf allocation in vegetation models with climate change. *Global Change Biology*, *25*(12), 4008–4021. https://doi.org/10.1111/gcb.14814

Trugman, A. T., Anderegg, L. D. L., Wolfe, B. T., Birami, B., Ruehr, N. K., Detto, M., Bartlett, M. K., & Anderegg, W. R. L. (2019). Climate and plant trait strategies determine tree carbon allocation to leaves and mediate future forest productivity. *Global Change Biology.*, *25*, 3395–3405. https://doi.org/10.1111/gcb.14680

Trugman, A. T., Detto, M., Bartlett, M. K., Medvigy, D., Anderegg, W. R. L., Schwalm, C., Schaffer, B., & Pacala, S. W. (2018). Tree carbon allocation explains forest drought-kill and recovery patterns. *Ecology Letters*, *21*(10), 1552–1560. https://doi.org/10.1111/ele.13136

van der Walt, S., Colbert, S. C., & Varoquaux, G. (2011). The NumPy array: A structure for efficient numerical computation. *Computing in Science & Engineering*, *13*(2), 22–30. https://doi.org/10.1109/MCSE.2011.37

Venturas, M. D., Sperry, J. S., & Hacke, U. G. (2017). Plant xylem hydraulics: What we understand, current research, and future challenges: Plant xylem hydraulics. *Journal of Integrative Plant Biology*, *59*(6), 356–389. https://doi.org/10.1111/jipb.12534

Venturas, M. D., Sperry, J. S., Love, D. M., Frehner, E. H., Allred, M. G., Wang, Y., & Anderegg, W. R. L. (2018). A stomatal control model based on optimization of carbon gain versus hydraulic risk predicts aspen sapling responses to drought. *New Phytologist.*, *220*, 836–850. https://doi.org/10.1111/nph.15333

Venturas, M. D., Todd, H. N., Trugman, A. T., & Anderegg, W. R. L. (2021). Understanding and predicting forest mortality in the western United States using long-term forest inventory data and modeled hydraulic damage. *New Phytologist*, *230*(5), 1896–1910. https://doi.org/10.1111/nph.17043

Vicente-Serrano, S. M., Beguería, S., & López-Moreno, J. I. (2010). A multiscalar drought index sensitive to global warming: The standardized precipitation evapotranspiration index. *Journal of Climate*, *23*(7), 1696–1718. https://doi.org/10.1175/2009JCLI2909.1

Virtanen, P., Gommers, R., Oliphant, T. E., Haberland, M., Reddy, T., Cournapeau, D., Burovski, E., Peterson, P., Weckesser, W., Bright, J., van der Walt, S. J., Brett, M., Wilson, J., Millman, K. J., Mayorov, N., Nelson, A. R. J., Jones, E., Kern, R., Larson, E., … Vázquez-Baeza, Y. (2020). SciPy 1.0: Fundamental algorithms for scientific computing in Python. *Nature Methods*, *17*(3), 261–272. https://doi.org/10.1038/s41592-019-0686-2

Von Humboldt, A., & Bonpland, A. (2010). *Essay on the geography of plants*. University of Chicago Press.

Walker, A. P., Beckerman, A. P., Gu, L., Kattge, J., Cernusak, L. A., Domingues, T. F., Scales, J. C., Wohlfahrt, G., Wullschleger, S. D., & Woodward, F. I. (2014). The relationship of leaf photosynthetic traits—V_{cmax} and J_{max}—to leaf nitrogen, leaf phosphorus, and specific leaf area: A meta-analysis and modeling study. *Ecology and Evolution*, *4*(16), 3218–3235. https://doi.org/10.1002/ece3.1173

Walker, A. P., De Kauwe, M. G., Bastos, A., Belmecheri, S., Georgiou, K., Keeling, R. F., McMahon, S. M., Medlyn, B. E., Moore, D. J. P., Norby, R. J., Zaehle, S., Anderson-Teixeira, K. J., Battipaglia, G., Brienen, R. J. W., Cabugao, K. G., Cailleret, M., Campbell, E., Canadell, J. G., Ciais, P., … Zuidema, P. A. (2021). Integrating the evidence for a terrestrial carbon sink caused by increasing atmospheric CO_2. *New Phytologist*, *229*(5), 2413–2445. https://doi.org/10.1111/nph.16866

Wang, Y., Sperry, J. S., Anderegg, W. R. L., Venturas, M. D., & Trugman, A. T. (2020). A theoretical and empirical assessment of stomatal optimization modeling. *New Phytologist*, *227*(2), 311–325. https://doi.org/10.1111/nph.16572

Wu, Z., Ahlström, A., Smith, B., Ardö, J., Eklundh, L., Fensholt, R., & Lehsten, V. (2017). Climate data induced uncertainty in model-based estimations of terrestrial primary productivity. *Environmental Research Letters*, *12*(6), 064013.

Yuen, K. K. (1974). The two-sample trimmed t for unequal population variances. *Biometrika*, *61*(1), 165–170.

SUPPORTING INFORMATION

Additional supporting information can be found online in the Supporting Information section at the end of this article.

How to cite this article: Quetin, G. R., Anderegg, L. D. L., Boving, I., Anderegg, W. R. L., & Trugman, A. T. (2023). Observed forest trait velocities have not kept pace with hydraulic stress from climate change. *Global Change Biology*, *29*, 5415–5428. https://doi.org/10.1111/gcb.16847